

Effects of Earth's Oblateness on Black Hole Imaging Through Earth-Space and Space-Space VLBI

ADITYA TAMAR ¹, BEN HUDSON ² AND DANIEL C. M. PALUMBO ^{3,4}

¹*Department of Physics, National Institute of Technology, Karnataka, Surathkal, Mangalore-575025, India*

²*KISPE Space Systems Ltd, Farnborough, United Kingdom*

³*Center for Astrophysics | Harvard & Smithsonian, 60 Garden Street, Cambridge, MA 02138, USA*

⁴*Black Hole Initiative at Harvard University, 20 Garden Street, Cambridge, MA 02138, USA*

ABSTRACT

Earth-based Very Long Baseline Interferometry (VLBI) has made rapid advances in imaging black holes. However, due to the limitations imposed on terrestrial VLBI by the Earth's finite size and turbulent atmosphere, it is imperative to have a space-based component in future VLBI missions. Herein, this paper investigates the effect of the Earth's oblateness, also known as the J_2 effect, on orbiters in Earth-Space and Space-Space VLBI. The paper provides an extensive discussion on how the J_2 effect can directly impact orbit selection for black hole observations and how through informed choices of orbital parameters, the effect can be used to the mission's advantage, a fact that has not been addressed in existing space-VLBI investigations. We provide a comprehensive study of how the orbital parameters of several current space VLBI proposals will vary specifically due to the J_2 effect. For black hole accretion flow targets of interest, we have demonstrated how the J_2 effect leads to modest increase in shorter baseline coverage, filling gaps in the (u, v) plane. Subsequently, we construct a simple analytical formalism that allows isolation of the impact of the J_2 effect on the (u, v) plane without requiring computationally intensive orbit propagation simulations. By directly constructing (u, v) coverage using the J_2 affected and invariant equations of motion, we obtain distinct coverage patterns for M87* and Sgr A* that show extremely dense coverage on short baselines as well as long term orbital stability on longer baselines.

Keywords: Artificial satellites (68), Supermassive Black Holes (1663); Very long baseline interferometry (1769);

1. INTRODUCTION

The field of radio astronomy, in particular very long baseline interferometry (VLBI), has made rapid advances in the field of black hole imaging, stimulated primarily by the observations of the Event Horizon Telescope (EHT) collaboration. The images of M87* (EHT 2019a) and Sgr A* (EHT 2022) provide a novel means to access the strong-field regime of black holes and enable direct probes of the magnetic field structures in the inner accretion flow through the polarization of synchrotron radiation (Event Horizon Telescope Collaboration et al. 2021a,b). Observations with lower frequency arrays such as the GMVA continue to improve our understanding of black hole accretion and jet launching (Lu et al. 2023) as well.

However, it is important to note that the EHT, and its immediate successor, the next generation EHT (ngEHT) (Johnson et al. 2023; Doleman et al. 2023; Ayzenberg et al. 2023) are Earth-based networks of observing stations. This has direct physical implications on the scientific value of the observed data. For example, the maximum length of a baseline that can be obtained is constrained by the diameter of the Earth. (EHT 2019b) and the observing frequency has to be chosen so as to ameliorate the effects of the Earth's atmosphere (Event Horizon Telescope Collaboration et al. 2019; Raymond et al. 2021).

It is therefore apparent that in order to continue improving the resolution and the Fourier plane (hereafter (u, v)) coverage, future VLBI missions targeting black hole astrophysics must have a space-based component. Indeed, there have been several recent mission concept studies in this domain (Andrianov et al. 2021; Johnson et al. 2021; Likhachev et al. 2022; Rudnitskiy et al. 2023; Kudriashov et al. 2021a; Roelofs et al. 2023; Kudriashov et al. 2021a; Kurczynski

et al. 2022; Trippe et al. 2023; Hudson et al. 2023). The space missions can be a single orbiter working in tandem with a ground based station to produce very long baselines, in turn leading to very high angular resolution. However, in this case one would still have to deal with effects of Earth’s atmosphere. The other alternative is of space-only VLBI that contains several orbiters forming baselines with one another, wherein deciding an appropriate formation geometry is a key task, encompassing both astrodynamics and VLBI site optimisation. Herein, one would eliminate any corrupting effects due to the Earth’s atmosphere.

In this paper, we provide a detailed investigation of how one realistic astrodynamical effect, namely the effect of Earth’s oblateness on an orbiter’s motion (the so-called J_2 effect), impacts the (u, v) coverage for observing M87* and Sgr A* using both Earth-Space and Space-Space VLBI. The choice of these sources is to develop a linear trajectory of improvement over the existing observations of the EHT. Now, it is a reasonable question to ask why specifically the J_2 effect is being studied when sophisticated orbit propagation models are already being used for space VLBI mission studies. These models include not just the J_2 effect, but also effects of air drag, dynamics of the upper atmosphere and so on (Vallado 2006). The reason for specifically investigating the J_2 effect is due to its peculiar nature wherein by an informed choice of related orbital parameters, the effect can be used to one’s *advantage*, as compared to being a “corrupting” influence on our observations. In particular, choices of orbital parameters informed by analysing the J_2 effect will lead to a significant impact for calculations related to the fuel budget of the mission, a non-trivial factor in mission design.

Keeping all of these factors in mind, the paper studies the J_2 effect on the (u, v) coverage using analytical tools developed in astrodynamical literature that model this effect for the orbiter’s motion. Since we are directly using the analytic expressions, the framework is much less computationally expensive than sophisticated orbit propagation models, while also providing insights into how such physical effects can impact black hole observations through a space-VLBI component. The layout of the paper is as follows: In Section 2 we provide an accessible introduction to the J_2 effect, its effect on orbital parameters and how the effect can be used to one’s advantage when selecting orbits to maximise scientific output from the coverage of the (u, v) in observing M87* and Sgr A*. In Section 3 we provide a detailed discussion of how the orbital parameters of existing VLBI missions with a space-based components are affected by the J_2 effect. In addition, a brief discussion is provided on the effect’s impact on the visibility domain signature of a photon ring modelled as an infinitesimally thin ring of unit flux. In Section 4 a novel analytic formalism is developed that describes the (u, v) coverage in terms of equations of motion of two space-based orbiters in relative motion of one another, namely the chief and the deputy. In Section 5 the relative motion is studied without incorporating the J_2 effect and the corresponding features of the baseline coverage are studied for both M87* and Sgr A*. In Section 6, the J_2 effect is incorporated through a linearisation scheme in the equations of motion and the corresponding (u, v) coverage for the same two black holes is studied. In Section 7, the equations of motion that produce orbits which are invariant under the J_2 effect are used and the bounded relative motion is observed in the (u, v) plane as well. Finally, Section 8 provides the conclusion, as well as some potential avenues for future work. For the benefit of the reader, a tabulation of some of the terminology used in the paper has been provided in Table 9 in the Appendix.

2. INCORPORATING ASTRODYNAMICS CONSIDERATIONS INTO VLBI: EFFECT OF EARTH’S GRAVITATIONAL FIELD VIA THE J_2 PERTURBATION

The Earth is essentially an oblate spheroid, and is flatter at the poles and bulging out at the equator (Schaub & Junkins 2003; Capderou 2014). As a consequence of this, the gravitational attraction towards a body orbiting the Earth is not directed towards the Earth’s centre of mass, as would be expected from classical Newtonian theory of gravitation. A common approach to model this effect on an orbiter is by expressing the gravitational potential in terms of spherical harmonics. If r, ϕ, λ are the satellite’s orbital radius, latitude, and longitude respectively, then the potential can be written as:

$$V(r) = \frac{\mu}{r} \sum_{l=0}^{\infty} \left(\frac{a_e}{r} \right)^l \sum_{m=0}^l P_{lm}(\sin \phi) (C_{lm} \cos m\lambda + S_{lm} \sin m\lambda), \quad (1)$$

wherein μ is the product of Newton’s gravitational constant and mass of Earth and a_e is the semi-major axis of Earth’s ellipsoid shape. The functions $P_{lm}(\cdot)$ are the associated Legendre functions of degree l and order m and C_{lm}, S_{lm} are spherical harmonic coefficients. Extremely accurate satellite measurements of these coefficients have been incorporated into the Joint Gravity Model 3 (JGM-3) developed by NASA (Tapley et al. 1996).

To understand the separate effects of the harmonics, one often splits this equation into three parts:

$$V = V_0 + V_1 + V_2, \quad (2)$$

where

$$V_0 = \frac{\mu}{r}, \quad (3)$$

$$V_1 = \frac{\mu}{r} \sum_{l=1}^{\infty} \left(\frac{a_e}{r} \right)^l P_{l0}(\sin \phi) C_{l0}, \quad (4)$$

$$V_2 = \frac{\mu}{r} \sum_{l=1}^{\infty} \left(\frac{a_e}{r} \right)^l \sum_{m=1}^l P_{lm}(\sin \phi) (C_{lm} \cos m\lambda + S_{lm} \sin m\lambda). \quad (5)$$

Here, V_0 is the classical potential when Earth is treated as a point mass. The term V_1 corresponds to the part of the potential which does not have longitudinal dependence and hence has $m = 0$. By defining

$$J_l \equiv -C_{l0}, \quad (6)$$

the ‘‘zonal’’ part of the potential is now written as:

$$V_1 = -\frac{\mu}{r} \sum_{l=1}^{\infty} \left(\frac{a_e}{r} \right)^l P_{l0}(\sin \phi) J_l. \quad (7)$$

The remaining part V_2 is dependent on the longitude.

For our purposes, we focus on Equation 7. It is the degree 2 zonal term, defined as J_2 in the equation, that models the contribution due to Earth’s oblateness and hence the change in dynamics arising due to it are sometimes known as the J_2 perturbation effect (King-Heele 1958). For this paper, we shall use the standard value of the J_2 coefficient (Sengupta 2003, hereafter S03)

$$J_2 = 1.082629 \times 10^{-3}. \quad (8)$$

As far as the effects of the J_2 perturbation are concerned, it is the dominant perturbing influence for orbiters in Low Earth Orbits (LEOs). Indeed, the Orbiter-Earth system can be modelled as a Keplerian 2-body problem and the dominant contribution of the J_2 terms can be investigated using Earth models such as the JGM-3. For LEO deployment, incorporation of J_2 effects via the JGM-3 model has a relatively better performance than the more widely used Simplified General Perturbation-4 (SGP4) model (Morales et al. 2019).

In the context of Earth-space VLBI, the motivation for studying its impact arises from the fact that several recent discussions of future missions have discussed placing stations in LEOs (Palumbo et al. 2019). At altitudes of around 800 km (which is in the LEO range), the J_2 perturbation is the dominant effect when compared to other realistic considerations such as atmospheric drag, solar radiation pressure (Alessi et al. 2018) and other electromagnetic effects (Marsden et al. 2001). For some related work on the non-trivial importance of J_2 on relative orbit motion, see Schweighart & Sedwick (2002) and for efforts on modelling orbits invariant to J_2 effects, see Schaub & Alfriend (2001); Schaub & Junkins (2003); Lee (2022).

2.1. Effect of J_2 perturbation on orbital parameters

For a given orbiter in space, there are 6 Keplerian orbital elements that can describe its behaviour: semimajor axis a , eccentricity e , inclination i , right ascension Ω , argument of perigee ω and mean anomaly M . Due to the J_2

perturbation, over a large number of orbits, the time evolution of these elements is affected as follows:

$$\dot{a} = 0, \quad \dot{e} = 0, \quad \dot{i} = 0, \quad (9)$$

$$\dot{\Omega} = -\frac{3}{2}nJ_2\left(\frac{R_e}{p}\right)^2 \cos i, \quad (10)$$

$$\dot{\omega} = \frac{3}{4}nJ_2\left(\frac{R_e}{p}\right)^2 (5 \cos^2 i - 1), \quad (11)$$

$$\dot{M} = n\left[1 + \frac{3}{4}\sqrt{1-e^2}J_2\left(\frac{R_e}{p}\right)^2 (3 \cos^2 i - 1)\right], \quad (12)$$

where

$$n = \sqrt{\frac{\mu}{a^3}}, \quad p = a\sqrt{1-e^2}. \quad (13)$$

and the ‘‘overdot’’ represents the time derivative of the corresponding parameters. Now the longitude Ω , inclination i and latitude θ form a 3 – 1 – 3 Euler angle system (S03). Moreover, considering long-term variation in orbital parameters over a large number of orbits, only effects of $\dot{\omega}$ are felt so we approximate (S03)

$$\dot{\theta} \approx \dot{\omega}, \quad (14)$$

thereby ignoring the effects of the harmonics of the true anomaly f . This approximation is valid for mission cycles of space VLBI missions such as Millimetron, which has an expected 10 year cycle of operation (Lazio et al. 2020).

To get a better understanding on how the orbital elements evolve over time, we can integrate the Equations 10, 11 and 12 assuming initial values Ω_0 , ω_0 and M_0 respectively. Note that due to Equation 9, the inclination i in this framework does not have time dependence. One obtains the following expressions:

$$\Omega(t) = \left(-\frac{3}{2}nJ_2\left(\frac{R_e}{p}\right)^2 \cos i\right)t + \Omega_0, \quad (15)$$

$$\omega(t) = \left(\frac{3}{4}nJ_2\left(\frac{R_e}{p}\right)^2 (5 \cos^2 i - 1)\right)t + \omega_0, \quad (16)$$

$$M(t) = \left(n\left[1 + \frac{3}{4}\sqrt{1-e^2}J_2\left(\frac{R_e}{p}\right)^2 (3 \cos^2 i - 1)\right]\right)t + M_0. \quad (17)$$

For future reference, we also note the approximate relation between true anomaly ν and mean anomaly:

$$\nu = M + (2e - \frac{1}{4}e^2) \sin M + \frac{5}{4}e^2 \sin 2M + \frac{13}{12}e^3 \sin 3M + \mathcal{O}(e^4). \quad (18)$$

Upon differentiating this relation, and assuming $\dot{e} = 0$ as in the case for J_2 's effect, we get:

$$\dot{\nu}_{J_2} = \dot{M} \left[1 + (2e - \frac{1}{4}e^2) \cos M + \frac{5}{2}e^2 \cos 2M + \frac{13}{4}e^3 \cos 3M\right]. \quad (19)$$

For the choice of orbits given in Table 1 (justification for which is provided in the following section), the variation of Ω, ω for a time period of 1 day and 1 month are tabulated in Table 2. The J_2 effect is apparent here. For example, the choice for ω for the Equatorial HEO is chosen to maximise the coverage of M87* but the parameter has variability even over a single day, and it only increases with time. This causes variation in the coverage of M87* that can be achieved, as will be demonstrated in subsequent sections. As another example, the effect of the so-called ‘‘critical/magic inclination’’ of $i = 63.4^\circ$ for the Molniya orbit is apparent since there is no time variation in ω . Such an inclination has been known in astrodynamics literature (for example, see Sabatini et al. (2008)) for some time, with Molniya orbits

Orbit Elements	700 km Sun-Sync	Equatorial HEO	Molniya Orbit
Semi-major axis (a) [km]	7078	14000	26600
Eccentricity (e)	0	0.50	0.74
Inclination (i) [°]	97.4	0.0	63.4
Right Ascension (Ω) [°]	0*	0	0
Argument of Perigee (ω) [°]	0	187	270
Period [hours]	1.7	4.6	12.0

Table 1. Keplerian elements of three prospective Earth orbits for a space-based interferometer. *Right ascension of a Sun-synchronous orbit must be selected based on launch date and relative Sun position.

being used for satellite orbits since the 1960’s [Allan \(1971\)](#). The numerical value of this inclination is obtained as follows:

$$\dot{\omega} = 0 \Rightarrow (5 \cos^2 - 1) = 0 \Rightarrow i = \cos^{-1}(1/\sqrt{5}) = 63.4^\circ. \quad (20)$$

Therefore, suitable modifications/extensions of the Molniya orbit for maximising the coverage of a particular source (just like we did for Equatorial HEO) can be used to counteract the variation in source coverage that might arise from the J_2 effect on orbital parameter ω .

2.2. Orbit Selection

As with many aspects of space system design, the orbit is often a trade-off between what is most desirable to meet the scientific objectives and the feasibility from a mission analysis perspective. Orbit selection will affect many aspects of the mission including power generation, thermal environment, communications and radiation exposure, to name a few. The effects on these factors must be carefully balanced through orbit selection to ensure the system can successfully meet the primary objectives and operate safely in the space environment.

For VLBI, orbit selection is primarily a geometrical consideration to achieve sufficient (u, v) coverage and resolution when observing the target astronomical sources. Considering a single space telescope observing in collaboration with ground-based stations, angular resolution will be driven by the maximum altitude of the orbit as increasing the baseline length is required to improve resolution. For VLBI imaging dense (u, v) coverage is required to increase the fidelity of the generated images. This is achieved by varying the baseline length throughout observations, therefore operating at a range of altitudes for a space-based system. Rapid (u, v) coverage is also desirable as the radio emitting environment of black holes is highly variable over short timescales. To capture the dynamic behaviour of supermassive black holes, coverage should be achieved in the shortest observation time possible (see analysis in [Roelofs et al. \(2023\)](#)). For an orbiting antenna, this encourages the selection of an orbit with a short time period (i.e. high orbital velocity) to sample a range of (u, v) points in as short a time as possible.

For this study a number of commonly used Earth orbits are evaluated in terms of their benefits from a VLBI and mission analysis perspective. The subset of orbits selected for analysis is by no means comprehensive but provide a good example of the trade-offs which must be resolved and the effect of the J_2 perturbation on the mission and subsequently, the VLBI observations. Table 1 contains the three analysed orbits with their respective Keplerian elements. Fig. 1 depicts the configurations in the Earth Centered Inertial (ECI) frame. The ECI frame $(\hat{X}, \hat{Y}, \hat{Z})$ is such that (\hat{X}, \hat{Y}) span the equatorial plane of the Earth, \hat{Z} is along the North pole and \hat{X} is along the vernal equinox. The origin of the system is at the Earth’s centre. This is analogous to the right-handed Cartesian co-ordinate system used in VLBI for specifying positions of antennas in an array ([Thompson et al. 2017](#)).

Now, depending on the specific objectives of the mission, the J_2 perturbation on right ascension and argument of perigee can either be beneficial or detrimental. For VLBI, careful selection of orbital elements could result in the nodal and apsidal precession being advantageous for the observation of supermassive black hole targets.

A Sun-synchronous orbit is a good example of a LEO that makes use of the J_2 perturbation on the right ascension of the ascending node. Many Earth-observing satellites observing at optical wavelengths require consistent lighting of specific targets. Sun-synchronous orbits make use of the nodal precession due to the J_2 perturbation to rotate the right ascension of the orbit so that the position of the Sun with respect to the orbital plane is constant throughout the year. The inclination and semi-major axis of a Sun-synchronous orbit are selected such that the nodal precession is equal to

Orbit	Orbital Parameter	Initial Value	Value after 1 day	Value after 1 month
700 km Sun-Sync	Ω	0°	0.32043°	9.7464°
700 km Sun-Sync	ω	0°	-1.14077°	-34.6985°
Equatorial HEO	Ω	0°	-0.84788°	-25.7898°
Equatorial HEO	ω	187°	188.696°	238.58°
Molniya	Ω	0°	-0.17416°	-5.29747°
Molniya	ω	270°	270°	270.002°

Table 2. Variation of orbital elements Ω and ω due to the J_2 effect after 1 day and 1 month

the rate of the Earth’s rotation about the Sun. For VLBI observations this is highly beneficial. Due to the stringent sensitivity requirements on VLBI interferometers, it is highly likely that space-based VLBI systems will require cooling of the receiver electronics to very low temperatures, depending on the frequency selected, as discussed in [Gurvits et al. \(2022\)](#). Like many space telescopes (e.g. James Webb), this may require all observations to be conducted away from the solar direction to simplify thermal control onboard. Maintaining the Sun in a constant position with respect to the orbital plane would simplify operations of the spacecraft drastically. A 700 km altitude has been selected for this orbit as this keeps the spacecraft outside of the Inner Van Allen Belt which begins to affect spacecraft electronics at higher altitudes. One notes that the use of a Sun-synchronous orbit for VLBI observations is one example of how careful orbit selection can make use of the orbit precession due to the Earth’s oblateness in a beneficial way.

An equatorial, Highly Elliptic Orbit (HEO) has been selected to demonstrate the apsidal precession effects of the J_2 perturbation. Having an inclination of 0° maximises the rate of change of the argument of perigee. The semi-major axis and eccentricity have been derived by selecting a perigee altitude of 700 km (the same as the Sun-synch) and an apogee of 21000 km (half of the Molniya) to provide a variation in (u, v) coverage from the other two orbits. The argument of perigee has been calculated to maximise coverage of M87*. As with the Molniya orbit, the increased apogee altitude compared to the Sun-synch provides a longer baseline to a ground-based station and thus, finer angular resolution. Unlike the Molniya, the period of this orbit is only ~ 4.5 hours providing more rapid (u, v) coverage as the spacecraft completes a full revolution of the Earth in almost a third of the time.

Molniya orbits were first designed to provide long periods of coverage over high latitudes, as opposed to the coverage typically offered by traditional communications satellites in Geostationary Earth Orbit (GEO). In order to achieve this, the orbit has a high eccentricity to increase the period of time spent over the target region. As has been discussed, apsidal precession due to the J_2 perturbation results in rotation of the argument of perigee over time. To combat this, the Molniya orbit makes use of a 63.4° inclination which results in zero apsidal precession. This is generally referred to as a frozen orbit as some perturbation effects have been cancelled out through the orbital element selection. This feature, along with the orbit’s large altitude variation (hence baseline variation), makes it of particular interest for this study.

Fig. 2, Fig. 3 and 4 depicts the (u, v) coverage achieved by each configuration for 7 day observations of M87* and Sgr A*. Observations are conducted at 345 GHz, with a single ground station, in this case the Large Millimeter Telescope (LMT) in Mexico. Observation could however be conducted with any ground-based antenna and still produce the same high-level (u, v) coverage features which are described below. As stated in [Roelofs et al. \(2023\)](#), this is the target frequency of the next generation EHT (ngEHT). For these simulations, each scan is conducted for 5 minutes, the average length of measurements conducted by the EHT in the observations of M87* (see [EHT \(2019b\)](#)). The instrument duty cycle is 10 minutes, providing 5 minutes between the end of one scan and the start of the next. The exact duty cycle of a space-based instrument will depend on many factors such as power requirements, data processing and storage, thermal conditions and observation of calibration sources. However, the general pattern of the (u, v) coverage remains consistent regardless of the duty cycle and it is simply the density of the coverage that will vary.

The variations in the orbits selected can be clearly seen in their respective (u, v) coverages of M87* and Sgr A*, shown in Fig. 2, Fig. 3 and 4. As expected, the finest resolution of $5.1 \mu\text{as}$ is achieved by the Molniya orbit configuration as it has the largest apogee of the three designs. However, due to the long period of this orbit (12 hours), the (u, v) coverage is very sparse compared to the Sun-synchronous and equatorial alternatives which complete 7.5 and 2.5 more revolutions about the Earth, respectively, in the same time. As M87* is at a fairly low declination, the (u, v) coverage of the equatorial HEO is less varied in the v -plane than the alternative, inclined orbits.

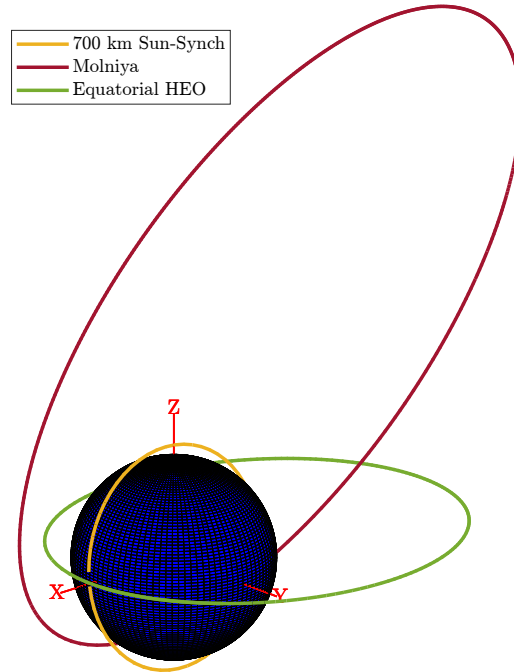


Figure 1. Analysed orbit configurations plotted in the ECI reference frame.

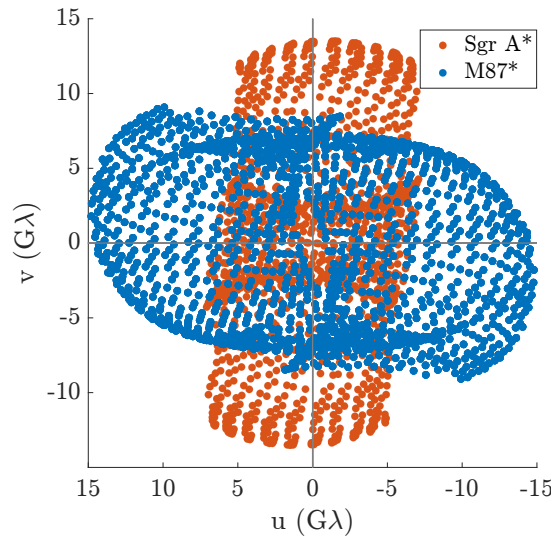


Figure 2. (u, v) coverage achieved by Sun-synchronous orbit configuration with the Large Millimeter Telescope (LMT), observation at 345 GHz.

All three configurations clearly demonstrate the benefits of space-based VLBI stations. The improvement in angular resolution is considerable compared to the $25 \mu\text{as}$ achieved by the EHT in its M87* and Sgr A* observations (see [EHT \(2019b\)](#), [EHT \(2022\)](#)). The Sun-synchronous orbiter produces a far denser (u, v) coverage and a resolution of $20.8 \mu\text{as}$ for M87*. The increased altitude of the equatorial HEO exhibits a resolution of $6.9 \mu\text{as}$, an improvement on the EHT by almost a factor of 5. These results were achieved by a simple interferometer of only two elements, the orbiter and the ground-based LMT. Denser coverage would be possible for observations with many more ground stations, even for the sparsely populated Molniya orbiter (u, v) plot. The long baselines achieved by the equatorial HEO and the Molniya orbit configurations also introduce the possibility of probing the first order photon ring of M87*. [Johnson et al. \(2020\)](#) showed that that the interferometric signature of the black hole is dominated by the photon ring contribution beyond

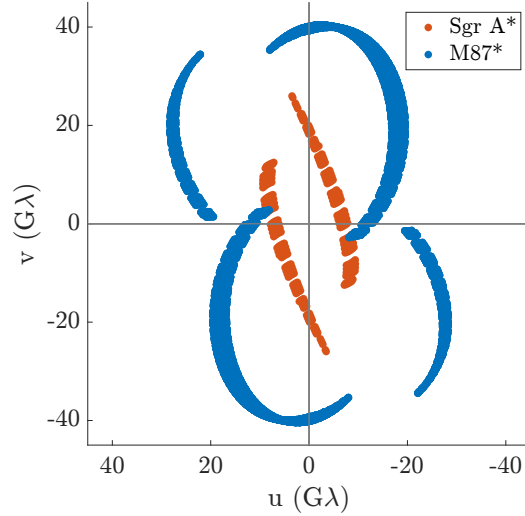


Figure 3. (u, v) coverage achieved by Molniya orbit configuration with the Large Millimeter Telescope (LMT), observation at 345 GHz.

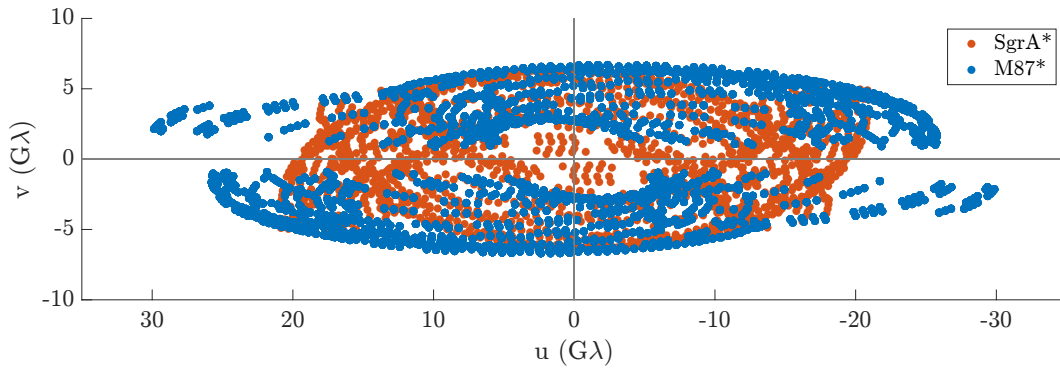


Figure 4. (u, v) coverage achieved by equatorial HEO configuration with the Large Millimeter Telescope (LMT), observation at 345 GHz.

~ 20 $G\lambda$ and that the sub-mm interferometric signatures of Sgr A* and M87* should be dominated by the photon ring contribution. Detection of the signature on very long baselines can allow one to estimate the angular diameter of the photon rings, from which uniquely robust and accurate tests of strong gravity and general relativity can be performed.

As is demonstrated in Fig. 2, Fig. 3 and 4, the (u, v) coverage of a radio source is dependent on the geometry of the orbit design. It is therefore possible to optimise the orbit configuration to maximise visibility and coverage of a certain source. The investment required to fund a future space-based VLBI mission will be significant and therefore the system will need to be highly versatile to justify the cost. Optimisation for observation of a single source will not be desirable. Changing the shape and orientation of an orbit can be an expensive orbit transfer. Conducting plane change maneuvers for varying inclination and right ascension are particularly demanding and often completely impractical in terms of the required propellant. The relative right ascension of the source with respect to the orbital plane will vary throughout the year due to the nodal and apsidal precession caused by J_2 . This natural variation can be used to change the visibility that the space-based element of the interferometer has of different sources.

Therefore, precession due to J_2 should be considered when designing orbit configurations to optimise coverage of certain sources. The equatorial HEO was selected to maximise the rate of apsidal precession to illustrate this approach. Fig. 5 depicts the precession of this orbit across a 12 month period. The argument of perigee changes by 183° due to the J_2 perturbation in a single year. The initial argument of perigee was selected to maximise the baseline length achieved for observations of M87*. The resolution of Sgr A* that would be achieved is $\sim 70\%$ of that for M87*. In this

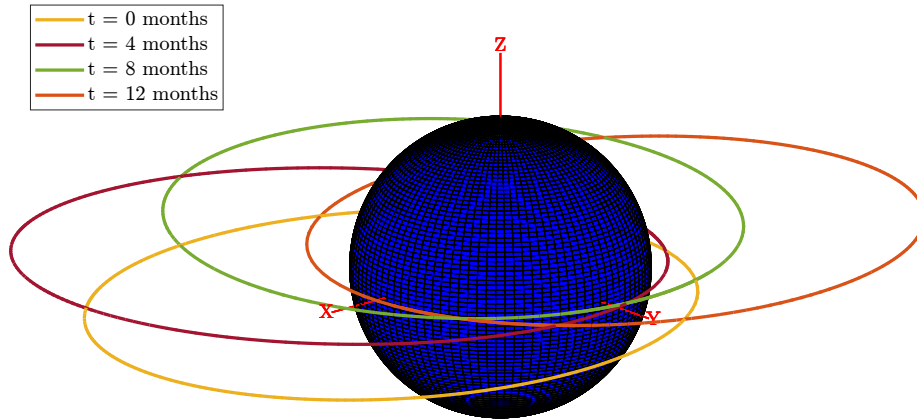


Figure 5. Equatorial HEO precession due to the J_2 perturbation across a 12 month period.

configuration, 8 months after the initial conditions the effect of the J_2 perturbation results in the resolution achieved during observations of Sgr A* improving from $9.8 \mu\text{as}$ to $8.0 \mu\text{as}$.

This highlights one of the disadvantages of the Molniya configuration and other frozen orbit types. By cancelling out the J_2 perturbation on right ascension and argument of perigee, the natural precession effects cannot be used to vary coverage of different sources. However, as a consequence, sometimes months would pass between the optimal observation times for different sources. It is however likely that this would be acceptable for a mission that would have a lifetime of at least 5 years. Scheduling with ground based arrays would need to be carefully conducted such that observations could take place at the optimal time. The orbit configuration of a space-based station can therefore be designed such that the natural perturbations due to J_2 are advantageous for the observation of radio sources and the operation of the spacecraft platform itself. However, ignoring the apsidal and nodal precession effects would likely result in an unfavourable geometry for certain sources that could have otherwise been avoided.

3. INVESTIGATING J_2 EFFECTS IN EXISTING EARTH-SPACE AND SPACE-VLBI PROPOSALS

Recently, there have been several mission concept studies in literature that have investigated the scientific merits of having a space-based VLBI station (Fromm et al. 2021; Roelofs et al. 2023; Rudnitskiy et al. 2022; Likhachev et al. 2022; Trippe et al. 2023; Kurczynski et al. 2022). These merits are intimately tied to the “cartography” of the (u, v) plots, with larger baselines implying higher angular resolution and shorter baselines improving the density of the (u, v) plane. Now, existing literature has explored in detail the scientific payoff of the increased coverage of the (u, v) plane with space VLBI. However, an extended discussion of how realistic astrodynamical effects acting on the orbiter can affect the (u, v) coverage has been lacking in these studies. Therefore, we now investigate how the J_2 perturbation specifically affects the orbital elements for the said mission concept studies. The focus is on those studies in which the relevant orbital parameters affected by J_2 have been explicitly provided.

Firstly, the parameters in Fromm et al. (2021) are investigated, wherein the authors devised an optimisation algorithm to observe Sgr A* over a 12h time period. The proposal involved a single space-based orbiter in a Medium Earth Orbit (MEO). The orbital parameters of the proposal, along with the change in values due to J_2 are given in Table 3.

We next investigate the proposal of Rudnitskiy et al. (2023). The authors considered deployment of two or more orbiters in near-Earth circular orbits so as to rapidly fill up the (u, v) plane. In echoing the results of Kudriashov et al. (2021b), it was stated that the choice of the Right Ascension of Ascending Node (RAAN) of -43° can provide similar (u, v) coverage for M87* and Sgr A*. Now, we know that RAAN (which is Ω in our notation) is indeed affected by the J_2 perturbation and based on the reasoning discussed earlier, the effect is expected to be much more prominent for near-Earth orbits. The variation of specifically the RAAN is shown in Table 4. It is therefore quite evident that the J_2 perturbation has a non-trivial effect on the RAAN for LEO deployments. Since the choice of RAAN was to observe a specific astronomical source (both M87* and Sgr A* for Ω_1 or just M87* for Ω_2), if the J_2 effect is not taken into account, there will be significant, unexpected variation in the visibility of target sources. This would effect the times at which the source is in view of the interferometer and the achievable variation in baseline length.

Orbital Parameter	Initial Value	Value after 12 h due to J_2
$a(\text{km})$	14,900	14,900
$i(^{\circ})$	67	67
e	0.5	0.5
$\Omega(^{\circ})$	46	45.8668
$\omega(^{\circ})$	70	69.9597
$M(^{\circ})$	330.373	1189.5

Table 3. Variation of orbital elements in [Fromm et al. \(2021\)](#) due to J_2 effect

Orb. Param.	Initial Value	After 12h	After 24h	After 12 days
$a(\text{km})$	7500	7500	7500	7500
e	0	0	0	0
$i(^{\circ})$	-61	-61	-61	-61
$\Omega_1(^{\circ})$	-43	-44.369	-45.739	-75.882
$\Omega_2(^{\circ})$	-82.29	-83.659	-85.0297	-115.173

Table 4. Variation of orbital elements in [Rudnitskiy et al. \(2023\)](#) due to J_2 effect. Here Ω_1 is the RAAN identified as giving similar (u, v) coverage for M87* and Sgr A*, while Ω_2 is to make Sgr A* the primary target.

Lastly, we consider the proposal of [Andrianov et al. \(2021\)](#) that considered the orbiter to be on a Highly Elliptical Orbit (HEO). Since the orbiter is in a HEO, the effect of J_2 is less prominent here. Nevertheless, the fact that the

Orb. Param.	Initial Value	After 10 days ($T1; J_2$)
$a(\text{km})$	165000	165000
e	0.939	0.939
$i(^{\circ})$	20.08	20.08
$\Omega(^{\circ})$	-3.583	-3.59198
$\omega(^{\circ})$	-92	-91.9837

Table 5. Variation of orbital elements in Orbit Type 1 of [Andrianov et al. \(2021\)](#) due to J_2 effect

proposal requires highly elliptical orbits, mitigation of the J_2 effect through orbit adjustment would lead to a non-trivial contribution to the fuel budget of the orbiter ([Lee 2022](#)). A notable feature of the study in [Andrianov et al. \(2021\)](#) is that they use the EGM96 Earth gravity model which does indeed take into account the non-central nature of the Earth’s gravitational field (including of course, the J_2 effect). This is similar to the Earth-space VLBI mission with RadioAstron being the space-based component [Kardashev et al. \(2013\)](#), which also took into account the non-central gravitational field of the Earth, along with perturbations due to the Moon and the Sun, noting that the presence of such factors “substantially complicated determination of the spacecraft orbit” ([Kardashev et al. 2013](#)).

From investigating the tables, several general inferences can be obtained. Firstly, the fact that the J_2 effect seems “negligible” in some cases is a consequence of the fact that the proposals discussed here considered orbiters in and around the Medium Earth Orbit (MEO), wherein the J_2 effect is smaller when compared to the LEO case. This is straightforward to infer from a physical sense because the farther the orbiter goes from the Earth, the lesser will be the effect of Earth’s gravitational field on it. Nevertheless, the J_2 effect does indeed contribute to the change in values of the orbital parameters which in several cases have been obtained from optimisation algorithms catered to observing a particular source, for example Sgr A* by [Fromm et al. \(2021\)](#). The fact that the J_2 effects reduce as the altitude of the orbiter increases is apparent. Therefore, since the primary impetus of going to larger baselines (and therefore to MEO and beyond) was to obtain sharpened angular resolution, it is important to investigate how specific perturbing

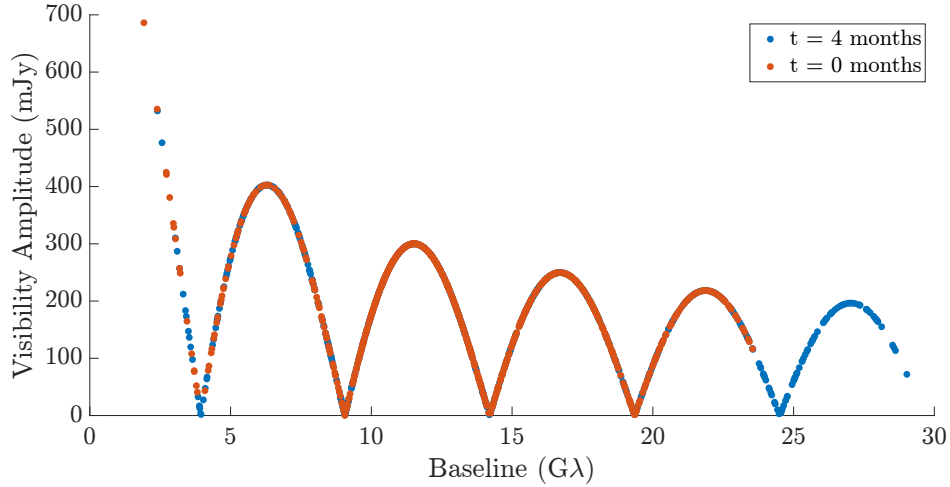


Figure 6. Interferometric signature of an infinitesimally-thin, circular ring, using parameters consistent with GRMHD simulations of M87*, demonstrating the variation in coverage caused by J_2 -induced orbit precession. Observations conducted over 15 days with same duty cycle and integration time parameters as used for Fig. 2, Fig. 3 and 4.

effects can influence these science goals. As far as LEO deployments are concerned, the importance of mitigating the J_2 perturbation is quite evident from Table 4.

The lessons drawn here are analogous to ones obtained from orbit determination studies for RadioAstron (Zakhvatkin et al. 2020). In addition to the evolution of the orbital parameters due to Earth’s gravitational field, it was noted that the solar radiation pressure was the main perturbing force affecting the orbiter’s motion. The modelling of the orbiter’s dynamics specifically taking this effect into account was crucial to studying the orbiter’s efficacy for conducting observations during the mission’s observing cycle. Therefore, one can envision that the J_2 effect can play a similar role in selecting orbits for LEO deployments of space VLBI missions.

3.1. The J_2 effect and photon ring observations

The high resolution observations of a black hole photon ring is one of the prime targets for future Earth-space and space-only VLBI observations (Johnson et al. 2020; Fish et al. 2020; Gralla et al. 2020; Kurczynski et al. 2022; Hudson et al. 2023). Indeed, one of the primary motivations for putting an orbiter into space for VLBI observations is to obtain baselines which are much longer than the ones possible using solely Earth-based stations. Keeping this in mind, it is imperative to investigate whether the J_2 effect impacts the observations of the photon ring.

To obtain a handle on these effects, we attempt to model the changes in the (u, v) plane due to the presence of the J_2 effect directly into photon ring observations in the visibility domain. In this domain, the interferometric signature $V(u)$ of an infinitesimally thin, uniform circular ring for a diameter d (measured in radians), observed on (u, v) -distances u (measured in wavelengths), is given by the zeroth order Bessel function of the first kind:

$$V = J_0(\pi du). \quad (21)$$

This ring has a unit total flux. Fig. 6 depicts the variation in coverage of a model photon ring about M87* due to the J_2 perturbation on the equatorial HEO interferometer configuration. On an Equatorial HEO, the inclusion of the J_2 effect leads to a preferable increase in the maximum baseline length achieved, after only 4 months of precession. The density of coverage over the shorter baselines is however reduced. The precession of different orbit configurations would no doubt result in a more drastic variation in the baseline coverage of the interferometer over time. The equatorial HEO example does however show that an appreciable difference in the interferometric signature can be observed due to the precession of the orbit. Therefore, this must be considered when planning observations of such a mission as depending on the current rotation of the right ascension about the equator, the baseline range achievable will vary.

4. INCORPORATING EQUATIONS OF MOTION OF ORBITERS INTO THE (u, v) SPACE

In radio interferometry and therefore in VLBI as well, the standard method to judge the efficacy of a baseline for various scientific goals is to investigate the coverage in the so-called (u, v) space (Thompson et al. 2017). Since the astrodynamics effects, in particular the Earth’s oblateness being discussed here, directly impact the equations of motion

of the orbiter, one requires a set of equations that directly map these equations to the coverage in the (u, v) plane. The astrodynamical considerations become all the more important for space-only VLBI observations since the astrodynamical effects would now affect *each and every* orbiter in a potentially distinct manner (based on the orbiter design, orbital parameters etc.), as compared to a simple Earth-Space VLBI deployment of a single orbiter. Therefore, it is even more important for space VLBI to have a mapping that allows for a suitable translation between astrodynamical effects and the associated consequences on the (u, v) plane.

For this paper, we shall consider the case of two orbiters in relative motion with one another, thereby forming a space-only baseline. In borrowing nomenclature from astrodynamics (S03), one orbiter is labelled as the Chief and the other orbiter is the Deputy. The equations of motion are modelled for the motion of the Deputy relative to that of the Chief. The analysis proceeds as follows.

We require two main co-ordinate systems, namely the ECI frame discussed earlier and the Local Vertical Local Horizontal (LVLH) frame which has the origin at the orbiting satellite (S03). Now, if (H, δ) are the hour-angle and declination respectively of the astrophysical source under observation, and λ is the observing wavelength, the (u, v, w) co-ordinates used in interferometry can be obtained from the components (X, Y, Z) components in the ECI frame by:

$$\begin{pmatrix} u \\ v \\ w \end{pmatrix} = \frac{1}{\lambda} \begin{pmatrix} \sin H & \cos H & 0 \\ -\sin \delta \cos H & \sin \delta \sin H & \cos \delta \\ \cos \delta \cos H & -\cos \delta \sin H & \sin \delta \end{pmatrix} \begin{pmatrix} X \\ Y \\ Z \end{pmatrix}. \quad (22)$$

For applications in VLBI, we only require the (u, v) co-ordinates since the contributions from the w co-ordinate are considered negligible, which arises from the assumption that the field of the source being synthesised is not too large (see Chapter 3 of Thompson et al. (2017) for an extended discussion on this matter). Therefore, we shall focus only on (u, v) and the corresponding equations are:

$$\begin{aligned} u &= \frac{1}{\lambda}(X \sin H + Y \cos H), \\ v &= \frac{1}{\lambda}(-X \sin \delta \cos H + Y \sin \delta \sin H + Z \cos \delta). \end{aligned} \quad (23)$$

Now, let \vec{r}_c be the position vector components of the chief in the ECI system:

$$\vec{r}_c = X_c \hat{X} + Y_c \hat{Y} + Z_c \hat{Z}, \quad (24)$$

and let the corresponding components in the LVLH frame be (X_{c0}, Y_{c0}, Z_{c0}) . Three of its orbital elements Ω, i and θ form a 3 – 1 – 3 Euler system ($\Omega - i - \theta$) and so the aforementioned components of its position vector in the ECI frame can be written in terms of the LVLH components using a directional cosine matrix (S03):

$$\begin{pmatrix} X_c \\ Y_c \\ Z_c \end{pmatrix} = \begin{pmatrix} \cos \theta_c \cos \Omega_c - \sin \theta_c \cos i_c \sin \Omega_c & -\sin \theta_c \cos \Omega_c - \cos \theta_c \cos i_c \sin \Omega_c & \sin i_c \sin \Omega_c \\ \cos \theta_c \sin \Omega_c + \sin \theta_c \cos i_c \cos \Omega_c & -\sin \theta_c \sin \Omega_c + \cos \theta_c \cos i_c \cos \Omega_c & -\sin i_c \sin \Omega_c \\ \sin \theta_c \sin i_c & \cos \theta_c \cos i_c & \cos i_c \end{pmatrix} \begin{pmatrix} X_{c0} \\ Y_{c0} \\ Z_{c0} \end{pmatrix}. \quad (25)$$

Here θ_c, i_c, Ω_c are the latitude, inclination and right ascension respectively for the chief. Expanding the equation, we get:

$$\begin{aligned} X_c &= (\cos \theta_c \cos \Omega_c - \sin \theta_c \cos i_c \sin \Omega_c)X_{c0} + (-\sin \theta_c \cos \Omega_c - \cos \theta_c \cos i_c \sin \Omega_c)Y_{c0} + (\sin i_c \sin \Omega_c)Z_{c0}, \\ Y_c &= (\cos \theta_c \sin \Omega_c + \sin \theta_c \cos i_c \cos \Omega_c)X_{c0} + (-\sin \theta_c \sin \Omega_c + \cos \theta_c \cos i_c \cos \Omega_c)Y_{c0} + (-\sin i_c \sin \Omega_c)Z_{c0}, \\ Z_c &= (\sin \theta_c \sin i_c)X_{c0} + (\cos \theta_c \cos i_c)Y_{c0} + (\cos i_c)Z_{c0}. \end{aligned} \quad (26)$$

If we now define (X_d, Y_d, Z_d) as the position vector components of the deputy in the ECI frame, we can define its (u, v) co-ordinates as in Equation 4. Then, using an analogous expression for the chief, we can define

$$\begin{aligned} u &\equiv u_d - u_c = \frac{1}{\lambda}((X_d - X_c) \sin H + (Y_d - Y_c) \cos H), \\ v &\equiv v_d - v_c = \frac{1}{\lambda}(-(X_d - X_c) \sin \delta \cos H + (Y_d - Y_c) \sin \delta \sin H + (Z_d - Z_c) \cos \delta). \end{aligned} \quad (27)$$

We now write this equation in the LVLH frame. In this frame, suppose the components of the separation vector between the chief and deputy are given by:

$$X_{d0} - X_{c0} = x, \quad Y_{d0} - Y_{c0} = y, \quad Z_{d0} - Z_{c0} = z. \quad (28)$$

Then, using Equation 26 for the chief, and exactly the same construction for the deputy (since both are in the LVLH frame, and Ω, i, θ transform any general vector from the ECI to the LVLH frame, the angles would be the same for both the chief and the deputy), substituting in Equation 27 along with Equation 28 for the difference in the position vector components, we get our main equations:

$$\begin{aligned} u(\lambda) &= \frac{1}{\lambda} \left\{ \sin H \left[(\cos \theta_c \cos \Omega_c - \sin \theta_c \cos i_c \sin \Omega_c)x + (-\sin \theta_c \cos \Omega_c - \cos \theta_c \cos i_c \sin \Omega_c)y \right. \right. \\ &+ (\sin i_c \sin \Omega_c)z \left. \right] + \cos H \left[(\cos \theta_c \sin \Omega_c + \sin \theta_c \cos i_c \cos \Omega_c)x + (-\sin \theta_c \sin \Omega_c + \cos \theta_c \cos i_c \cos \Omega_c)y \right. \\ &\left. \left. - (\sin i_c \sin \Omega_c)z \right] \right\}, \\ v(\lambda) &= \frac{1}{\lambda} \left\{ -\sin \delta \cos H \left[(\cos \theta_c \cos \Omega_c - \sin \theta_c \cos i_c \sin \Omega_c)x + (-\sin \theta_c \cos \Omega_c - \cos \theta_c \cos i_c \sin \Omega_c)y \right. \right. \\ &+ (\sin i_c \sin \Omega_c)z \left. \right] + \cos \delta \left[(\cos \theta_c \sin \Omega_c + \sin \theta_c \cos i_c \cos \Omega_c)x + (-\sin \theta_c \sin \Omega_c + \cos \theta_c \cos i_c \cos \Omega_c)y \right. \\ &\left. \left. - (\sin i_c \sin \Omega_c)z \right] + \cos \delta \left[(\sin \theta_c \sin i_c)x + (\cos \theta_c \cos i_c)y + (\cos i_c)z \right] \right\}. \quad (29) \end{aligned}$$

The Equations 29, explicitly derived to the best of our knowledge for the first time, will be the main tools used to incorporate astrodynamics effects into space-only VLBI. In particular, one notices that due to the mapping between the equation of motion of an orbiter, given by (x, y, z) , and the (u, v) plane, the realistic effects incorporated in the former can now be reflected in the latter.

Lastly, one can note that since the origin of the chief's LVLH frame has $(x = y = z = 0)$, the (u, v) co-ordinates are $(0, 0)$. Thus, the (u, v) plane is "centered" on the chief orbiter's LVLH frame.

5. EQUATIONS FOR RELATIVE MOTION FOR CHIEF AND DEPUTY: NO J_2 EFFECT

Let ρ be the relative orbit radius. Then, under the assumption of having a circular reference orbit and no perturbing forces, the relative equations of motion are given by the Hill-Clohessey-Wiltshire (HCW) Equations (Schaub & Junkins 2003):

$$\begin{aligned} \ddot{x} - 2n_c \dot{y} - 3n_c^2 x &= 0, \\ \ddot{y} + 2n_c \dot{x} &= 0, \\ \ddot{z} + n_c^2 z &= 0 \end{aligned} \quad (30)$$

where n_c is the mean motion for the chief obtained by substituting the orbital parameter r_c of the chief into r in 13. Notice that the (x, y) motion is decoupled from the z -motion. The former can be modelled as coupled harmonic oscillator while the latter can be modelled as a harmonic oscillator.

For bounded motion with relative orbit radius ρ and initial conditions such that the orbits trace a circle in the $(y - z)$ plane, and assuming no offset in the the x and y direction, solution to these equations is given by:

$$\begin{aligned} x(t) &= \rho \cos(n_c t + \alpha), \\ y(t) &= -2\rho \sin(n_c t + \alpha), \\ z(t) &= 2\rho \cos(n_c t + \alpha). \end{aligned} \quad (31)$$

Orb. Param.	Value
$a_c(\text{km})$	7000
e_c	0
$i_c(^{\circ})$	35
$\theta_c(^{\circ})$	0
$\Omega_c(^{\circ})$	0

Table 6. Orbital Parameters of the Chief

5.1. (u, v) plots

We now construct the (u, v) plots using the equations of motion given in Equation 31. The choice of parameters are given in Table 6. The numerical values are inspired from the ones given in S03 and the form of the solutions is obtained using the equations in Ginn (2006). In addition, we consider the mean relative orbital radius ρ and the offset α to be

$$\rho = 25\text{km}, \quad \alpha = 0. \quad (32)$$

Lastly, we consider observations to be at 345 GHz. Substituting all of these parameters into the Equations 29, we obtain the (u, v) tracks shown in Figure 7. It can be noticed that the baselines obtained through this formalism are not

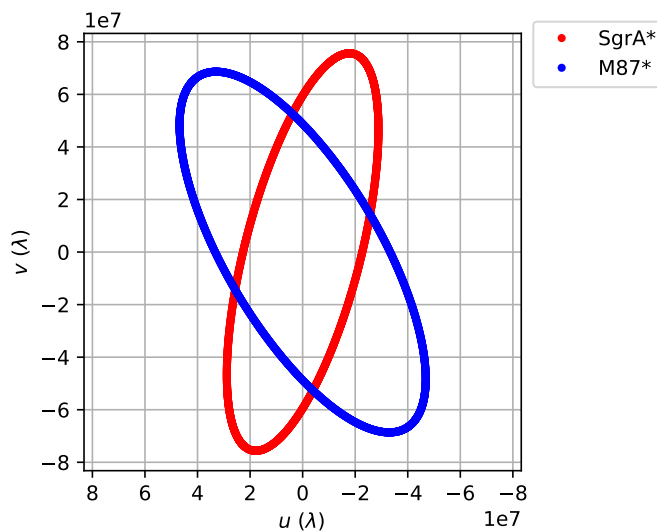


Figure 7. (u, v) coverage of M87* and Sgr A* at $f = 345$ GHz using HCW equations for a time period of 6 months.

large enough for high angular resolution observations required for say resolving the photon ring (Johnson et al. 2020). This should be expected because the HCW equations were obtained using a linearisation argument because of which the order of separation between the chief and deputy (10’s of km) has to be much less than the semi-major axis of the chief (1000’s of km). Therefore, while changing the values of ρ to higher values by “brute force” will give “bigger” ellipses in the (u, v) plane, it would not be faithful to the physical basis of the HCW solutions. Nevertheless, one can still obtain such elliptical plots in the (u, v) plane using a modified set of equations that make the orbits invariant to certain effects of the J_2 perturbation. This will be discussed in later sections.

6. EQUATIONS FOR RELATIVE MOTION FOR CHIEF AND DEPUTY: INCORPORATING J_2 CORRECTIONS THROUGH LINEARISATION

We now discuss how the effects of J_2 perturbation can be incorporated using linearisation of the equations of motion. The formalism for the same has been provided in Schweighart (2001); Ginn (2006) and it has been provided in the

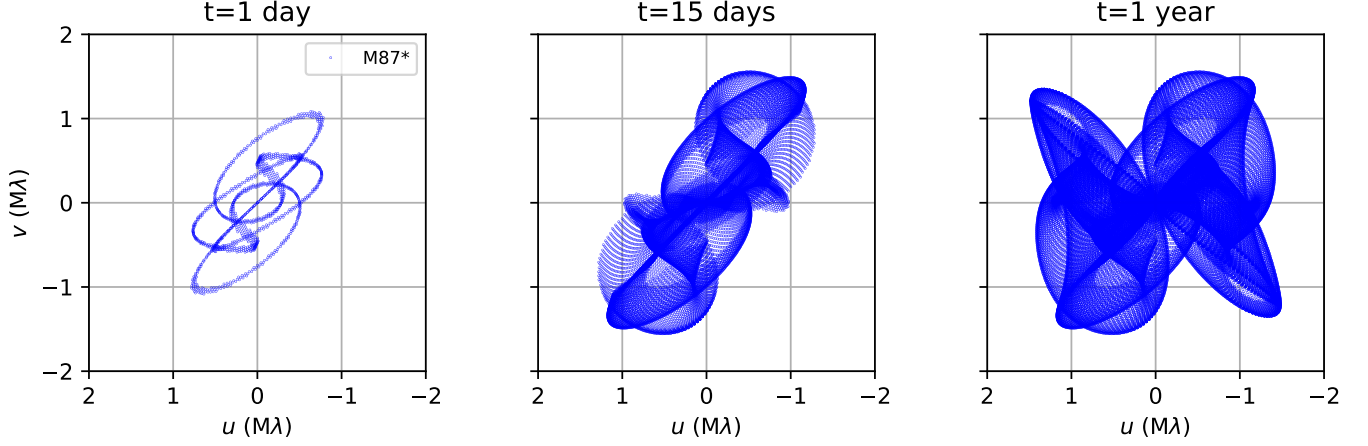


Figure 8. (u, v) plots for M87* J_2 effects and cross-track drift corrections. The time periods are, from left to right, 1 day, 15 days and 1 year.

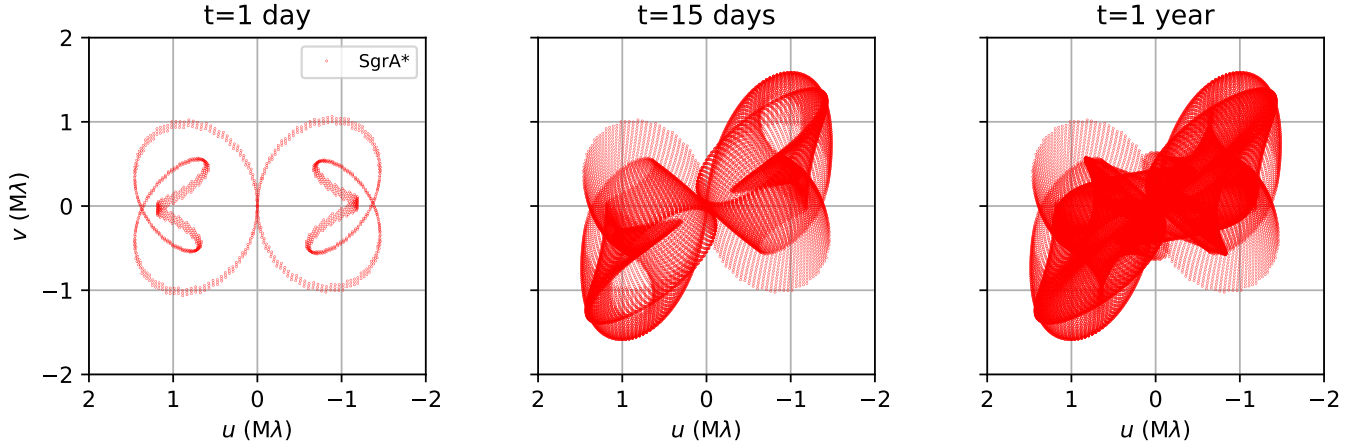


Figure 9. (u, v) plots for Sgr A* including J_2 effects and cross-track drift corrections. The time periods are, from left to right, 1 day, 15 days and 1 year.

Appendix. In the subsequent sections, we discuss the applications of the formalism to obtain (u, v) plots of M87* and Sgr A*.

6.1. (u, v) plots

The (u, v) plots M87* are given in Figure 8 whilst for Sgr A* are given in Figure 9. Several inferences can be drawn. Firstly, the plots show a remarkably rich and distinctive character based on the black hole that is being observed, namely M87* and Sgr A*. In particular, these plots follow directly from the equations of motion without use of any “optimisation” procedures, thereby allowing us to directly capture the impact of the J_2 effect on the (u, v) coverage. Secondly, as time passes, the plots become increasingly dense and thus provide dense (u, v) on short baselines, a desired feature of space-VLBI missions (Fish et al. 2020). We note that in order to generate these plots, only a small sample of the data points have been used that were generated by the choice of the sampling rate. For time periods of 1 day, 15 days and 1 year, we used 700, 15,000 and 30,000 data points respectively. This choice was governed largely by requiring a reasonable processing time to generate and process the plots in a higher resolution. It has been verified that utilisation of all the plot points leads to a modest increase in filling (u, v) in the “North-West” and “South-East” parts of the plot for M87* and “North-South” parts for Sgr A*. In addition, there is an overall increase in the coverage density. Nevertheless, the existing plots still demonstrate the key scientific takeaway of rapidly increasing density over

medium-length baselines providing a rich geometric coverage pattern generated primarily by the J_2 effect. The extremely dense coverage over shorter baselines introduces the possibility of having an “ALMA-like” flying formation of orbiters in space that can have much longer integration times and observe every single day throughout the year without having to mitigate intra-day variability in weather. As another potential avenue, one can consider a “hybrid” mission wherein one one hand, the chief and/or the deputy can work in an “Earth-Space” mode, forming long baselines allowing high angular resolution images of the photon ring, as discussed in the earlier sections on Earth-space VLBI. On the other hand, the the orbiters can operate in a “Space-only” more wherein the relative baselines formed between them as part of a formation can allow for observations of large-scale structure pertaining to black hole accretion. While providing a detailed description of a mission design based on these principles is beyond the scope of this paper, the results here indicate that in both of these considerations, the J_2 effect can turn out to be advantageous in not only providing dense (u, v) coverage, but also aiding in suitable orbit selection.

7. EQUATIONS FOR RELATIVE MOTION FOR CHIEF AND DEPUTY: J_2 INVARIANT ORBITS

There have been several investigations into obtaining suitable orbital parameters such that the motion of the orbiter is unaffected by the J_2 perturbation (Schaub & Alfriend 2001; Lee 2022). In this section, we shall largely be following the discussion given in Lee (2022).

The J_2 perturbation *independently* affects the latitude θ and the RAAN Ω and so finding J_2 invariant orbits boils down to searching for orbital parameters that can minimise their secular change over time, as given in Equations 10, 11 and 12. Suppose we consider the motion of the chief. If one has to minimise the effect of the J_2 perturbation on the chief, then the following equation must be solved

$$\dot{\theta}_c = \dot{\omega}_c + \dot{M}_c = 0. \quad (33)$$

Now, for the subsequent discussion, we shall consider the chief to be in a circular orbit, and so

$$e_c = 0. \quad (34)$$

Upon substituting the expressions from 11 and 12 into 33, and using the circular orbit condition 34 we get (Lee 2022):

$$\dot{\theta} = \frac{3}{2} J_2 n_c \left(\frac{R_e}{a_c} \right)^2 (4 \cos^2 i_c - 1) = 0. \quad (35)$$

Since the terms outside the bracket are constants, this equation can only be satisfied when the term in the bracket is 0:

$$4 \cos^2 i_c - 1 = 0 \Rightarrow i_c = \pm 60^\circ. \quad (36)$$

Thus, if one wishes to minimise the change in latitude for the chief in a circular orbit, that can be achieved by having it at an inclination angle of 60° . It is important to note that this result holds for *all* altitudes of the chief satellite. Note that this is analogous to our earlier calculation in Equation 20 on having an inclination of 63.4° that minimised $\dot{\omega}$ for the Molniya orbit.

Now, if the change in latitude due to the J_2 perturbation has to be minimised, we have:

$$\dot{\theta}_d = \dot{M}_d + \dot{\omega}_d = 0. \quad (37)$$

Using once again the Equations 11 and 12, we get (Lee 2022):

$$\dot{\theta}_d = \frac{3}{4} J_2 n_d \left(\frac{R_e}{p_d} \right)^2 \left[(5 + 3\sqrt{1 - e_d^2}) \cos^2 i_d - (\sqrt{1 - e_d^2} + 1) \right] = 0. \quad (38)$$

Solving for i_d , we have the condition (Lee 2022):

$$i_d = \pm \cos^{-1} \left(\sqrt{\frac{1 + \sqrt{1 - e_d^2}}{5 + 3\sqrt{1 - e_d^2}}} \right). \quad (39)$$

Thus for a given value of the eccentricity of the deputy, the inclination that minimises the J_2 perturbation can be obtained by solving the Equation 39. One can also do similar calculations for minimising the RAAN, which as we mentioned earlier has an independent effect on the equations of motion, but in this paper we focus on the effects of minimising the change in latitude, postponing the RAAN based discussion to a future work.

Now, minimising the drift in θ has a direct impact on the fuel budget of the mission. Under an impulsive control scheme that aims to maintain constant relative motion between the deputy and chief during the mission lifetime, the so-called ΔV requirement for the scheme for latitude correction, exercised after one orbit, is given by (Lee 2022):

$$\Delta V_{\dot{\theta}} = \frac{a_c}{3} [(\dot{\omega}_d - \dot{\omega}_c) + (\dot{M}_d - \dot{M}_c)]. \quad (40)$$

Thus, if both $\dot{M}_c + \dot{\omega}_c = 0$ and $\dot{M}_d + \dot{\omega}_d = 0$ hold, we have

$$\Delta V_{\dot{\theta}} = 0, \quad (41)$$

and so additional fuel will not be dispensed to maintain relative motion. Similar considerations apply for minimising the RAAN (Lee 2022).

7.1. (u, v) plots for J_2 invariant orbits

We now obtain the (u, v) plots for J_2 invariant relative motion using suitable parameter substitution in Equation 29.

Firstly, for the chief we consider the parameters given in 7. The mean anomaly M_c has not been mentioned since it does not play a role in the subsequent discussions. The choice of $i_c = 60^\circ$ implies that there would be no change in

$a_c(km)$	e_c	i_c°	θ_{c0}°	Ω_{c0}°
7000	0	60	0	0

Table 7. Orbital Parameters of the Chief for J_2 Invariant Orbits

the latitude θ_c over time. We thus assume:

$$\theta_c(t) \equiv \theta_{c0}, \quad \Omega_c(t) \equiv \Omega_{c0}. \quad (42)$$

Since the latitude and RAAN drift independently affect the relative motion under the J_2 effect, one can only design a configuration that minimises either one of them. Indeed, the equations to solve for inclinations that minimise the J_2 effect on RAAN are different than those for minimising the effect in the latitude (Lee 2022).

Lastly, we do allow for mean anomaly of the deputy to have a time dependence as per the Equation 17.

Now, following Lee (2022), the equation of motion of the deputy in the chief's frame, for the case that both chief and deputy have the same altitude, with the chief having a small eccentricity, modelled so that there is zero relative latitude drift, is:

$$\begin{aligned} x(t) &= -a_d \cos \left[M_d(t) \sqrt{1 - \left(\frac{1 - 5 \cos^2 i_d}{3 \cos^2 i_d - 1} \right)^2} \right], \\ y(t) &= 2a_d \sin \left[M_d(t) \sqrt{1 - \left(\frac{1 - 5 \cos^2 i_d}{3 \cos^2 i_d - 1} \right)^2} \right]. \end{aligned} \quad (43)$$

wherein $M_d(t)$ is governed by the Equation 17. For the conditions discussed here, the motion along z direction is negligible (Lee 2022) and so we assume

$$z(t) = 0. \quad (44)$$

We now describe in detail the choices for parameters of the deputy. Firstly, since the chief and deputy have to have the same altitude and hence the same semi-major axis, we have:

$$a_d = a_c = 7000\text{km}. \quad (45)$$

Next, we assume the deputy to have a small eccentricity of

$$e_d = 0.08, \quad (46)$$

and using Equation 39, we get the value for inclination to be (taking only the positive value):

$$i_d = 60.0066^\circ. \quad (47)$$

We choose the initial value of the mean anomaly to be

$$M_{d0} = 0^\circ, \quad (48)$$

so that at a later time t , we have:

$$\begin{aligned} M_d(t) &= \left(n_d \left[1 + \frac{3}{4} \sqrt{1 - e_d^2} J_2 \left(\frac{R_e}{p_d} \right)^2 (3 \cos^2 i_d - 1) \right] \right) t + M_{d0}, \\ &= \left(n_d \left[1 + \frac{3}{4} \sqrt{1 - e_d^2} J_2 \left(\frac{R_e}{p_d} \right)^2 (3 \cos^2 i_d - 1) \right] \right) t. \end{aligned} \quad (49)$$

Upon substituting the numerical values for the parameters, we get:

$$M_d^\circ(t) = 0.0618367^\circ t. \quad (50)$$

Then, using Equation 50 and substituting the value for i_d into Equation 43, we get the final equations of motion:

$$\begin{aligned} x(t) &= -7000 \cos(0.0618367^\circ t \times 0.08) = -7000 \cos(0.00494693^\circ t), \\ y(t) &= 14,000 \sin(0.00494693^\circ t). \end{aligned} \quad (51)$$

These are the final equations of motion that shall now be substituted into the (u, v) Equations 29.

7.2. (u, v) plots

The (u, v) plots for M87* and Sgr A* are given in Figure 10. The observation time is chosen to be 1 day at a sampling rate of 500s. The choice of observing frequency is $f = 345\text{GHz}$. The plots have distinctly different elliptical shapes as compared to the ones obtained without the J_2 effect from the HCW equations in Figure 7. Thus this at the very least establishes the fact that the J_2 effect in and of itself does impact the (u, v) coverage of the sources under consideration. More generally, The (u, v) plots look deceptively straightforward as standard VLBI plots for large baselines. However, the point we wish to convey with the plots is *precisely* that, which is to say that suitable choice of parameters which are specifically aimed at minimising the J_2 effect *can* give (u, v) plots which are suitable for VLBI investigations. As a particular example, if a space based VLBI mission that deploys antennas in LEOs takes a simplified approach of just specifying the orbital parameters of the antenna without taking into realistic effects such as the J_2 , there would a significant drift in the orbiter's motion if such effects are not taken into account, further affecting fuel budgets that would impact the mission cycle. While it is true that rigidity in the choice of orbital parameters might lead to certain compromises on the astronomical sources that can be observed, such considerations provide an impetus to investigate space-only VLBI optimisation software that does take into account realistic astrodynamical considerations. We wish to investigate these avenues in the near future.

8. CONCLUSION

The paper attempts to investigate in detail the effects of the Earth's oblateness, also known as the J_2 effect, on an Earth-Space and a Space-Space VLBI mission that aims to provide black hole images of the sources M87* and Sgr A*.

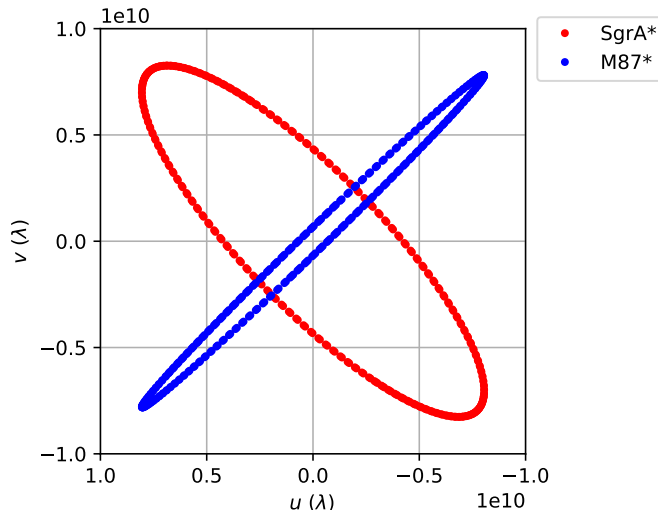


Figure 10. (u, v) coverage of M87* and Sgr A* using J_2 invariant equations of motion of Lee (2022) for a time period of 1 day.

An extensive study has been performed of several existing VLBI proposals in literature that investigated observing these sources using VLBI with a space-based component. In a similar vein, for the Earth-Space missions, a detailed discussion is provided on how an informed choice of orbital parameters based on isolating the J_2 effect can be used to one’s advantage in space mission design. For the Space-Space VLBI regime, the impact of the J_2 effect is studied using a simple, computationally accessible analytic framework that studies the relative motion of a chief orbiter and a deputy orbiter in relative motion. It was found that the J_2 effect leads to distinct patterns on the (u, v) plane for both M87* and Sgr A* which are extremely dense over short baselines, thereby potentially opening up an avenue of providing a dense filling of the (u, v) plane in space VLBI missions using just a couple of orbiters. Moreover, it was demonstrated that an informed choice of orbital parameters can also lead to bounded relative motion over longer baselines that is invariant under the J_2 perturbation.

8.1. Future Work

There is a smorgasbord of avenues that can be explored that cultivate a strong synergy between astrodynamical considerations and observations using space VLBI. For example, the impact/advantage of J_2 effect for making polarimetric observations of the photon ring using Earth-Space VLBI (Palumbo et al. 2023) can be explored that can highlight whether an informed choice of orbital parameters can lead to more robust observables in the presence of astrodynamical perturbations. In a similar vein, one can investigate the similar impact on closure quantities in space VLBI operations, which in our nomenclature would correspond to one chief and at least two deputy satellites for closure amplitudes and three deputies for closure phases. Herein, one can look at how a cluster of satellites (say 3), while operating under the J_2 effect, can lead to robust interferometric closure observables; the appropriate orbit selection for these has been studied in Marsden et al. (2001) and formation of orbits of such clusters including the J_2 perturbation effect has also been investigated Schweighart & Sedwick (2002). We note that the J_2 effect is even more important here since the most significant error when modelling relative orbits of a chief and deputy is due to the assumption that the Earth is spherical (Schweighart & Sedwick 2002).

In terms of developments focusing on developing an astrodynamical framework tailored to VLBI, one can envision a “dynamic” space-VLBI mission in which we utilise a suite of astrodynamical manoeuvres that can adjust the orbit parameters of the orbiter so as to optimise its coverage for several sources over a given mission cycle. For example, when an orbiter forms a baseline with an Earth-based station, the semi-major axis of the orbiter can be increased or decreased so as to investigate photon ring science and jet related structures respectively. Manoeuvres such as changing individual orbital parameters such as inclination, RAAN etc can also be performed to optimise pointing at a particular source of interest. A comprehensive discussion of such manoeuvres is given in Vallado (2006) and one can investigate whether taking advantage of the J_2 effect in the spirit of the discussion provided in the paper can help reduce the fuel budget for such missions. We expect to explore these avenues in the near future.

Lastly, the results of this paper suggest that an ambitious mission in the distant future of having an “ALMA-like”

configuration in space can be considered wherein the orbit selection informed by the J_2 effect can provide extremely dense (u, v) coverage over shorter baselines. Such orbiters, can also work in conjunction with other stations at faraway points like $L2$ to have very long baselines and thereby catering to observations of the black hole photon ring. This deployment can provide a VLBI network in space that is in principle similar to how ALMA currently operates with Earth-based stations to cater to a variety of scientific goals. We hope that the results of this paper would stimulate investigations into expanding the scientific scope of radio astronomy missions from space.

9. ACKNOWLEDGMENTS

A.T. acknowledges fruitful discussions with Kazunori Akiyama, Vincent Fish, Soung Sub Lee and Sascha Trippe. D.C.M.P. was supported by the Black Hole Initiative at Harvard University, which is funded by grants from the John Templeton Foundation (JTF-62286) and the Gordon and Betty Moore Foundation (GBMF-8273.01).

APPENDIX

A. THE J_2 EQUATIONS OF MOTION

The general equation of motion under the influence of the J_2 effect is given by:

$$\ddot{\vec{r}} = -\frac{\mu}{r^2} + J_2(\vec{r}) \equiv g(\vec{r}) + J_2(\vec{r}), \quad (\text{A1})$$

where

$$J_2(\vec{r}) = -\frac{3J_2\mu R_e^2}{2r^4} [(1 - 3\sin^2 i \sin^2 \theta)\hat{x} + (2\sin^2 i \sin \theta \cos \theta)\hat{y} + (2\sin i \cos i \sin \theta)\hat{z}]. \quad (\text{A2})$$

where \hat{x} points in the radial direction of the satellite's position vector, \hat{z} is perpendicular to the orbital plane and \hat{y} completes the orthogonal triad and points in the direction of motion of the satellite. For all our cases, we would consider a circular reference orbit of the chief ($r_{\text{ref}} \equiv r_c$) under the influence of the gravitational potential of the spherical Earth, and so the equation of motion of the reference orbit is given by:

$$\ddot{\vec{r}}_{\text{ref}} = g(\vec{r}_{\text{ref}}), \quad (\text{A3})$$

where $g(\vec{r})$ is the gravitational force due to a spherical Earth and the subscript ref implies that it is the force experienced by the chief in its frame. The equation of motion of the deputy is obtained by linearising the gravitational terms in A1 with respect to the reference orbit:

$$\ddot{\vec{r}} = g(\vec{r}) + \nabla g(\vec{r}) \cdot (\vec{r} - \vec{r}_{\text{ref}}) + J_2(\vec{r}_{\text{ref}}) + \nabla J_2(\vec{r}_{\text{ref}}) \cdot (\vec{r} - \vec{r}_{\text{ref}}), \quad (\text{A4})$$

where the ‘‘dot’’ implies dot product between the vectors. The gradient terms in the $(r - \theta - i)$ system are given by:

$$\begin{aligned} \nabla g(\vec{r}) &= \begin{pmatrix} \frac{2\mu}{r} & 0 & 0 \\ 0 & \frac{-\mu}{r} & 0 \\ 0 & 0 & \frac{-\mu}{r} \end{pmatrix}, \\ \nabla J_2 &= \frac{6\mu J_2 R_e^2}{r_{\text{ref}}^2} \begin{pmatrix} (1 - 3\sin^2 i \sin^2 \theta) & \sin^2 i \sin 2\theta & \sin 2i \sin \theta \\ \sin^2 i \sin 2\theta & -\frac{1}{2} - \sin^2 i (\frac{1}{2} - \frac{7}{4} \sin^2 \theta) & \frac{-\sin 2i \cos \theta}{4} \\ \sin 2i \sin \theta & \frac{-\sin 2i \cos \theta}{4} & -\frac{3}{4} - \sin^2 i (\frac{1}{2} + \frac{5}{4} \sin^2 \theta) \end{pmatrix}. \end{aligned} \quad (\text{A5})$$

Now, taking the motion with respect to the reference orbit, we have

$$\vec{x} = \vec{r} - \vec{r}_{\text{ref}}, \quad (\text{A6})$$

and since the reference orbit is rotating, with say angular velocity ω , the equation of motion, obtained by taking the double derivative of \vec{x} will have contributions from ω . From the known transformation in classical dynamics to a rotating co-ordinate system, we get:

$$\ddot{\vec{x}} = \ddot{\vec{r}} - \ddot{\vec{r}}_{\text{ref}} - 2\vec{\omega} \times \dot{\vec{x}} - \dot{\vec{\omega}} \times \vec{x} - \vec{\omega} \times (\vec{\omega} \times \vec{x}). \quad (\text{A7})$$

For a circular reference orbit,

$$\vec{\omega} = \sqrt{\frac{\mu}{r_{\text{ref}}^3}} \hat{z} \equiv n\hat{z}. \quad (\text{A8})$$

Finally, using Equation A4 into Equation A7, we get:

$$\ddot{\vec{x}} + 2\vec{\omega} \times \dot{\vec{x}} + \dot{\vec{\omega}} \times \vec{x} + \vec{\omega} \times (\vec{\omega} \times \vec{x}) = g(\vec{r}_{\text{ref}}) + \nabla g(\vec{r}_{\text{ref}}) \cdot \vec{x} + J_2(\vec{r}_{\text{ref}}) + \nabla J_2(\vec{r}_{\text{ref}}) \cdot \vec{x} - \ddot{r}_{\text{ref}}. \quad (\text{A9})$$

Next, we take into account further considerations that arise due to the presence of the J_2 dependent terms in Equation A9. The equation is a linearised equation of motion in which the term $\nabla J_2(\vec{r}_{\text{ref}})$ is not constant except for equatorial orbits. An approximate solution to take this into account is to time average the term:

$$\begin{aligned} \frac{1}{2\pi} \int_0^{2\pi} \nabla J_2(\vec{r}) d\theta &= \frac{\mu}{r^3} \begin{pmatrix} 4s & 0 & 0 \\ 0 & -s & 0 \\ 0 & 0 & -3s \end{pmatrix}, \\ s &= \frac{3J_2 R_e^2}{8r^2} (1 + 3 \cos 2i). \end{aligned} \quad (\text{A10})$$

Next, the effect of the J_2 force is that the perturbed satellite has a different period when compared to the case when the J_2 effect was absent. Due to this, the deputy drifts apart from the reference orbit and the linearised equations break down. To fix this, we take the time average of the “ J_2 -force” term as well:

$$\frac{1}{2\pi} \int_0^{2\pi} J_2(\vec{r}) d\theta = -n^2 r s \hat{x}. \quad (\text{A11})$$

This changes the reference orbit,

$$\ddot{\vec{r}}_{\text{ref}} = g(\vec{r}_{\text{ref}}) + \frac{1}{2\pi} \int_0^{2\pi} J_2(\vec{r}_{\text{ref}}) d\theta, \quad (\text{A12})$$

which in turn changes the angular velocity ω of the rotating co-ordinate system. The new velocity can be found from

$$\vec{\omega} \times (\vec{\omega} \times \vec{r}_{\text{ref}}) = g(\vec{r}_{\text{ref}}) + \frac{1}{2\pi} \int_0^{2\pi} J_2(\vec{r}_{\text{ref}}) d\theta, \quad (\text{A13})$$

that gives the new angular velocity as:

$$\vec{\omega} = n\sqrt{1+s} \hat{z} \equiv nc\hat{z}. \quad (\text{A14})$$

Thus, our final equation of motion that incorporates all these effects is given by:

$$\begin{aligned} \ddot{\vec{x}} + 2\vec{\omega} \times \dot{\vec{x}} + \dot{\vec{\omega}} \times \vec{x} + \vec{\omega} \times (\vec{\omega} \times \vec{x}) &= \nabla g(\vec{r}_{\text{ref}}) \cdot \vec{x} + J_2(\vec{r}_{\text{ref}}) \\ &+ \frac{1}{2\pi} \int_0^{2\pi} \nabla J_2(\vec{r}_{\text{ref}}) d\theta \cdot \vec{x} - \frac{1}{2\pi} \int_0^{2\pi} J_2(\vec{r}_{\text{ref}}) d\theta. \end{aligned} \quad (\text{A15})$$

A.1. Case II.A: including cross-track drift

As found by Schweighart, the solution to the equation of motion A15 for the components $\vec{x} = (x, y, z)$ of the relative separation vector is given by:

$$x(t) = (x_0 - \alpha) \cos(nt\sqrt{1-s}) + \frac{\sqrt{1-s}}{2\sqrt{1+s}} y_0 \sin(nt\sqrt{1-s}) + \alpha \cos(2nt\sqrt{1+s}), \quad (\text{A16})$$

$$y(t) = -\frac{2\sqrt{1+s}}{\sqrt{1-s}} (x_0 - \alpha) \sin(nt\sqrt{1-s}) + y_0 \cos(nt\sqrt{1-s}) + \frac{1+3s}{2(1+s)} \alpha \sin(2nt\sqrt{1+s}), \quad (\text{A17})$$

$$\begin{aligned} z(t) &= z_0 \cos(nt\sqrt{1+3s}) + \frac{z_0}{n\sqrt{1+3s}} \sin(nt\sqrt{1+3s}) \\ &+ \beta \left(\sqrt{1+s} \sin(nt\sqrt{1+3s}) - \sqrt{1+3s} \sin(nt\sqrt{1+s}) \right), \end{aligned} \quad (\text{A18})$$

wherein

$$\alpha = \frac{3J_2R_e^2}{8r_{\text{ref}}(3+5s)}(1 - \cos 2i_{\text{ref}}), \quad \beta = \frac{3J_2R_e^2 \sin 2i_{\text{ref}}}{4r_{\text{ref}}s\sqrt{1+3s}}, \quad (\text{A19})$$

and x_0, y_0, z_0 are the initial positions and \dot{x}_0, \dot{y}_0 and \dot{z}_0 are the initial velocities. For the case of no drift and offset in any direction, we have:

$$\dot{x}_0 = y_0 n \left(\frac{1-s}{2c} \right), \quad y_0 = -2ncx_0 + \frac{3nJ_2R_e^2(1 - \cos 2i_{\text{ref}})}{8kr_{\text{ref}}}. \quad (\text{A20})$$

Note that there is an error in Schweighart's Eq. 3.27 (Schweighart 2001) in that the term in the denominator of \dot{y}_0 has to be $8k$ instead of $8c$.

In the equations above, even though the J_2 effect has been incorporated, the orbiter still drifts apart from the reference orbit in the z direction. This can be seen as follows. Suppose we set the initial conditions to be

$$\begin{aligned} x_0 &= 0(\text{km}), & y_0 &= 0(\text{km}) & z_0 &= 0(\text{km}), \\ \dot{x}_0 &= 0((\text{km/s})), & \dot{y}_0 &= 0((\text{km/s})), & \dot{z}_0 &= 0((\text{km/s})). \end{aligned} \quad (\text{A21})$$

Then, the equation of motion in z direction is

$$z(t) = \beta \left(\sqrt{1+s} \sin(nt\sqrt{1+3s}) - \sqrt{1+3s} \sin(nt\sqrt{1+s}) \right). \quad (\text{A22})$$

For the orbital parameters of the chief given in 8, the drift in the z -direction is apparent in the Figure 11.

Orb. Param.	Value
$a_c(\text{km})$	7000
e_c	0
$i_c(^{\circ})$	35
$\theta_c(^{\circ})$	0
$\Omega_c(^{\circ})$	0

Table 8. Orbital Parameters of the Chief for demonstrating drift in z -direction.

For these given values, since $z(t) \neq 0$, the expression for $v(\lambda)$ contains a contribution from the $z(t)$ component. Thus, it fails to have stable, bounded motion thereby making it the (u, v) plane devoid of coherent tracks. A solution suitable for physical applications that attempts to fix this is given in the next subsection.

A.2. Case II.B: correcting cross-track drift

Schweighart (2001) identified that the normal component of the J_2 force causes the drift in the z -direction. This affects four out of the six orbital elements and by solving the equations that govern their time evolution, under the assumption of constant inclination, the time evolution of the orbital elements is given by (Schweighart 2001):

$$i(t) = i_0 - \frac{3\sqrt{\mu}J_2R_e^2}{2kr^{7/2}} \cos i \sin i \sin^2(2kt), \quad (\text{A23})$$

$$\Omega(t) = \Omega_0 - \frac{3\sqrt{\mu}J_2R_e^2}{2kr^{7/2}} \cos i \left[tk - \frac{\sin(2kt)}{2} \right], \quad (\text{A24})$$

$$\theta(t) = nct + \frac{3\sqrt{\mu}J_2R_e^2}{2kr^{7/2}} \cos^2 i \left[tk - \frac{\sin(2kt)}{2} \right], \quad (\text{A25})$$

where

$$k = nc + \frac{3\sqrt{\mu}J_2R_e^2}{2kr^{7/2}}. \quad (\text{A26})$$

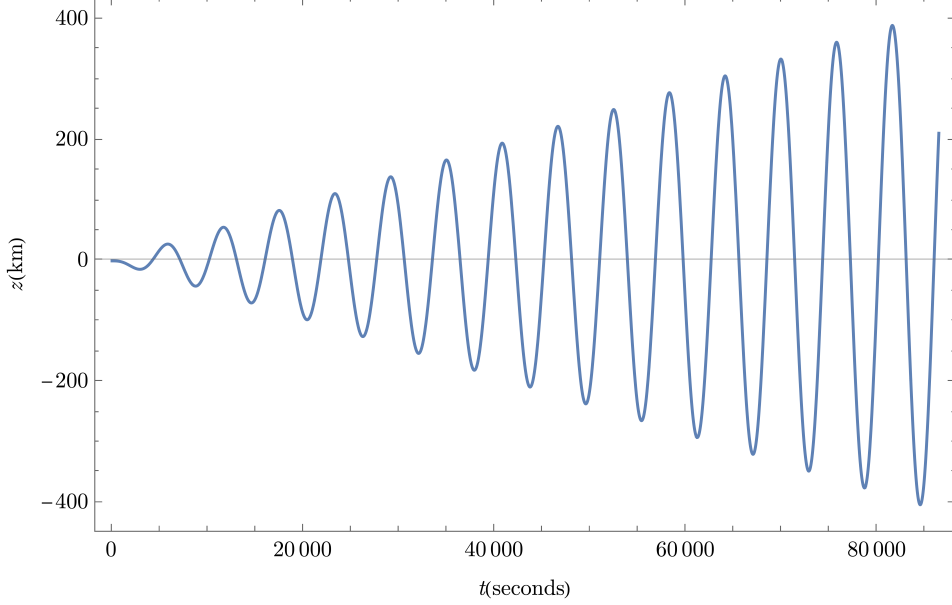


Figure 11. The drift in z direction from Schweighart's equations.

To fix the resultant drift, Schweighart added this component to the reference orbit in A12 as follows:

$$\ddot{\vec{r}}_{ref} = g(\vec{r}_{ref}) + \frac{1}{2\pi} \int_0^{2\pi} J_2(\vec{r}_{ref}) d\theta + \vec{J}_2(\vec{r}_{ref}) \cdot \hat{N}. \quad (\text{A27})$$

Now, both the perturbed and the reference orbiter have a drift in the longitude of the ascending node and thus the satellites will not drift apart.

The solution to the components $\vec{x} = (x, y, z)$ in this case is given by:

$$x(t) = (x_0 - \alpha_2) \cos(nt\sqrt{1-s}) + \frac{\sqrt{1-s}}{2\sqrt{1+s}} \dot{y}_0 \sin(nt\sqrt{1-s}) + \alpha_2 \cos(2kt), \quad (\text{A28})$$

$$y(t) = -\frac{2\sqrt{1+s}}{\sqrt{1-s}} (x_0 - \alpha_2) \sin(nt\sqrt{1-s}) + \dot{y}_0 \cos(nt\sqrt{1-s}) + \beta_2 \sin(2kt), \quad (\text{A29})$$

$$z(t) = z_0 \cos(nt\sqrt{1+3s}) + \frac{\dot{z}_0}{n\sqrt{1+3s}} \sin(nt\sqrt{1+3s}), \quad (\text{A30})$$

wherein

$$\alpha_2 = -\frac{3J_2 R_e^2 n^2 (3k - 2n\sqrt{1+s})}{8kr_{ref}(n^2(1-s) - 4k^2)} (1 - \cos 2i), \quad (\text{A31})$$

$$\beta_2 = -\frac{3J_2 R_e^2 n^2 (2k(2k - 3n\sqrt{1+s}) + n^2(3 + 5s))}{2k(n^2(1-s) - 4k^2)} 2k(n^2(1-s) - 4k^2)(1 - \cos 2i). \quad (\text{A32})$$

All other parameters have the same values as the previous case. Note that there is another (rather non-trivial) error in Schweighart's equations. Namely the equations for x and y were incorrectly written with y_0 instead of the corrected expression above that has \dot{y}_0 . This can be double checked with Ginn (2006). Curiously, the resultant plots made by Schweighart use the correct expressions (i.e using \dot{y}_0 instead of y_0).

B. NOTATION AND TERMINOLOGY

Since the results of the paper rely on the cross-fertilisation of astrodynamical and VLBI considerations, an accessible tabulation of the related terminology has been provided in Table 9.

Terminology	Description
Argument of Perigee (ω)	Orientation of the ellipse in the orbital plane (measured from the ascending node to the periapsis).
Baseline	Vector drawn between two telescopes observing the same source orthographically projected to the source.
Chief Orbiter	The primary orbiter in reference to which the motion of other orbiters is studied.
Deputy Orbiter	The orbiter moving relative to the primary orbiter. There can be several deputy orbiters moving in reference to a primary orbiter.
Eccentricity (e)	Elliptical shape of the orbit ($0 < e < 1$).
Earth Centered Inertial (ECI) Frame	Earth-centered coordinate system fixed with respect to the celestial sphere.
Local Vertical Local Horizontal (LVLH) frame	Spacecraft-centered coordinate system with respect to the nadir direction and the perpendicular local horizontal.
Hour Angle and Declination (H, δ)	The standard co-ordinates used to locate the position of an astronomical source on the celestial sphere.
Inclination (i)	Orientation of the orbit with respect to the equator.
J_2 effect	The effect on the dynamical motion of the body arising due to the oblateness of the Earth.
Mean Anomaly M	Fraction of an elliptical orbit's period that has elapsed since passing the periapsis.
Right Ascension of Ascending Node (Ω)	Intersection of the ascending direction of the orbit and the equator, with respect to the vernal equinox.
Semi-Major Axis (a)	Size of the orbit (average of the apoapsis and periapsis radii).
(u, v) coverage	The set of image-conjugate Fourier coefficients sampled by the baselines swept out by a set of telescopes during a given observations.
(3-1-3) Euler angle system	Orientation of a rigid body with respect to an inertial coordinate system, described by three rotation angles such that the order of rotation is done first for the "third" axis of the original system, then the "first" axis of the intermediate system and then finally on the "third" axis of the final transformed system.

Table 9. Terminology used in the paper

REFERENCES

- Alessi, E. M., Schettino, G., Rossi, A., & Valsecchi, G. B. 2018, *MNRAS*, 473, 2407, doi: [10.1093/mnras/stx2507](https://doi.org/10.1093/mnras/stx2507)
- Allan, R. R. 1971, *Celestial Mechanics*, 3, 320, doi: [10.1007/BF01231804](https://doi.org/10.1007/BF01231804)
- Andrianov, A. S., Baryshev, A. M., Falcke, H., et al. 2021, *MNRAS*, 500, 4866, doi: [10.1093/mnras/staa2709](https://doi.org/10.1093/mnras/staa2709)
- Ayzenberg, D., Blackburn, L., Brito, R., et al. 2023, arXiv e-prints, arXiv:2312.02130, doi: [10.48550/arXiv.2312.02130](https://doi.org/10.48550/arXiv.2312.02130)
- Capderou, M. 2014, *Handbook of Satellite Orbits From Kepler to GPS* (Springer International Publishing Switzerland)
- Doeleman, S. S., Barrett, J., Blackburn, L., et al. 2023, *Galaxies*, 11, 107, doi: [10.3390/galaxies11050107](https://doi.org/10.3390/galaxies11050107)
- EHT. 2019a, *Astrophysical Journal Letters*, 875, L1, doi: [10.3847/2041-8213/ab0ec7](https://doi.org/10.3847/2041-8213/ab0ec7)
- . 2019b, *Astrophysical Journal Letters*, 875, L2, doi: [10.3847/2041-8213/ab0c96](https://doi.org/10.3847/2041-8213/ab0c96)
- . 2022, *Astrophysical Journal Letters*, 930, L12, doi: [10.3847/2041-8213/ac6674](https://doi.org/10.3847/2041-8213/ac6674)
- Event Horizon Telescope Collaboration, Akiyama, K., Alberdi, A., et al. 2019, *ApJL*, 875, L3, doi: [10.3847/2041-8213/ab0c57](https://doi.org/10.3847/2041-8213/ab0c57)
- Event Horizon Telescope Collaboration, Akiyama, K., Algaba, J. C., et al. 2021a, *ApJL*, 910, L12, doi: [10.3847/2041-8213/abe71d](https://doi.org/10.3847/2041-8213/abe71d)
- . 2021b, *ApJL*, 910, L13, doi: [10.3847/2041-8213/abe4de](https://doi.org/10.3847/2041-8213/abe4de)
- Fish, V. L., Shea, M., & Akiyama, K. 2020, *Advances in Space Research*, 65, 821, doi: [10.1016/j.asr.2019.03.029](https://doi.org/10.1016/j.asr.2019.03.029)
- Fromm, C. M., Mizuno, Y., Younsi, Z., et al. 2021, *A&A*, 649, A116, doi: [10.1051/0004-6361/201937335](https://doi.org/10.1051/0004-6361/201937335)
- Ginn, J. S. 2006, Master's thesis, University of Texas at Arlington, USA
- Gralla, S. E., Lupsasca, A., & Marrone, D. P. 2020, *PhRvD*, 102, 124004, doi: [10.1103/PhysRevD.102.124004](https://doi.org/10.1103/PhysRevD.102.124004)
- Gurvits, L. I., Paragi, Z., Amils, R. I., et al. 2022, *Acta Astronautica*, 196, 314, doi: <https://doi.org/10.1016/j.actaastro.2022.04.020>
- Hudson, B., Gurvits, L. I., Wielgus, M., et al. 2023, *Acta Astronautica*, 213, 681, doi: <https://doi.org/10.1016/j.actaastro.2023.09.035>
- Johnson, M. D., Kovalev, Y. Y., Lisakov, M. M., et al. 2021, *ApJL*, 922, L28, doi: [10.3847/2041-8213/ac3917](https://doi.org/10.3847/2041-8213/ac3917)
- Johnson, M. D., Lupsasca, A., Strominger, A., et al. 2020, *Science Advances*, 6, doi: [10.1126/sciadv.aaz1310](https://doi.org/10.1126/sciadv.aaz1310)
- Johnson, M. D., Akiyama, K., Blackburn, L., et al. 2023, *Galaxies*, 11, 61, doi: [10.3390/galaxies11030061](https://doi.org/10.3390/galaxies11030061)
- Kardashev, N. S., Khartov, V. V., Abramov, V. V., et al. 2013, *Astronomy Reports*, 57, 153, doi: [10.1134/S1063772913030025](https://doi.org/10.1134/S1063772913030025)
- King-Heele, D. G. 1958, *Proc. R. Soc. Lond. A*, 247, 49, doi: [10.1098/rspa.1958.0169](https://doi.org/10.1098/rspa.1958.0169)
- Kudriashov, V., Martin-Neira, M., Barat, I., et al. 2021a, arXiv e-prints, arXiv:2105.06901, doi: [10.48550/arXiv.2105.06901](https://doi.org/10.48550/arXiv.2105.06901)
- Kudriashov, V., Martin-Neira, M., Roelofs, F., et al. 2021b, *Chinese Journal of Space Science*, 41, 211, doi: [10.3724/SP.J.0254-6124.2021.0202](https://doi.org/10.3724/SP.J.0254-6124.2021.0202)
- Kurczynski, P., Johnson, M. D., Doeleman, S. S., et al. 2022, in *Society of Photo-Optical Instrumentation Engineers (SPIE) Conference Series*, Vol. 12180, *Space Telescopes and Instrumentation 2022: Optical, Infrared, and Millimeter Wave*, ed. L. E. Coyle, S. Matsuura, & M. D. Perrin, 121800M, doi: [10.1117/12.2630313](https://doi.org/10.1117/12.2630313)
- Lazio, T. J. W., Briskin, W., Bouman, K., et al. 2020, arXiv e-prints, arXiv:2005.12767, doi: [10.48550/arXiv.2005.12767](https://doi.org/10.48550/arXiv.2005.12767)
- Lee, S. S. 2022, *Adv. Space Res.*, 69, 3502, doi: [10.1016/j.asr.2022.02.023](https://doi.org/10.1016/j.asr.2022.02.023)
- Likhachev, S. F., Rudnitskiy, A. G., Shchurov, M. A., et al. 2022, *MNRAS*, 511, 668, doi: [10.1093/mnras/stac079](https://doi.org/10.1093/mnras/stac079)
- Lu, R.-S., Asada, K., Krichbaum, T. P., et al. 2023, *Nature*, 616, 686, doi: [10.1038/s41586-023-05843-w](https://doi.org/10.1038/s41586-023-05843-w)
- Marsden, J., Koon, W., Murray, R., & Masdemont, J. 2001, *J2 dynamics and formation flight* (American Institute of Aeronautics and Astronautics), doi: [10.2514/6.2001-4090](https://doi.org/10.2514/6.2001-4090)
- Morales, J. J., Khalife, J., Cruz, U. S., & Kassas, Z. M. 2019, in *Proceedings of the 32nd International Technical Meeting of the Satellite Division of The Institute of Navigation (ION GNSS+ 2019)*, 2090–2099
- Palumbo, D. C. M., Doeleman, S. S., Johnson, M. D., Bouman, K. L., & Chael, A. A. 2019, *ApJ*, 881, 62, doi: [10.3847/1538-4357/ab2bed](https://doi.org/10.3847/1538-4357/ab2bed)
- Palumbo, D. C. M., Wong, G. N., Chael, A., & Johnson, M. D. 2023, *ApJL*, 952, L31, doi: [10.3847/2041-8213/ace630](https://doi.org/10.3847/2041-8213/ace630)
- Raymond, A. W., Palumbo, D., Paine, S. N., et al. 2021, *ApJS*, 253, 5, doi: [10.3847/1538-3881/abc3c3](https://doi.org/10.3847/1538-3881/abc3c3)
- Roelofs, F., Blackburn, L., Lindahl, G., et al. 2023, *Galaxies*, 11, 12, doi: [10.3390/galaxies11010012](https://doi.org/10.3390/galaxies11010012)
- Rudnitskiy, A. G., Mzhelskiy, P. V., Shchurov, M. A., Syachina, T. A., & Zapevalin, P. R. 2022, *Acta Astronautica*, 196, 29, doi: [10.1016/j.actaastro.2022.03.036](https://doi.org/10.1016/j.actaastro.2022.03.036)

- Rudnitskiy, A. G., Shchurov, M. A., Chernov, S. V., Syachina, T. A., & Zapevalin, P. R. 2023, arXiv e-prints, arXiv:2305.19072, doi: [10.48550/arXiv.2305.19072](https://doi.org/10.48550/arXiv.2305.19072)
- Sabatini, M., Izzo, D., & Bevilacqua, R. 2008, *Journal of Guidance Control Dynamics*, 31, 94, doi: [10.2514/1.30314](https://doi.org/10.2514/1.30314)
- Schaub, H., & Alfriend, K. T. 2001, *Celestial Mechanics and Dynamical Astronomy*, 79, 77, doi: [10.1023/A:1011161811472](https://doi.org/10.1023/A:1011161811472)
- Schaub, H., & Junkins, J. L. 2003, *Analytical Mechanics of Aerospace Systems* (American Institute of Aeronautics and Astronautics)
- Schweighart, S. A. 2001, Master's thesis, Massachusetts Institute of Technology, USA
- Schweighart, S. T., & Sedwick, R. J. 2002, *J. Guid. Control Dyn.*, 25, 1073, doi: [10.2514/2.4986](https://doi.org/10.2514/2.4986)
- Sengupta, P. 2003, Master's thesis, Texas A&M University, Texas, USA
- Tapley, B. D., Watkins, M. M., Ries, J. C., et al. 1996, *J. Geophys. Res.*, 101, 28,029, doi: [10.1029/96JB01645](https://doi.org/10.1029/96JB01645)
- Thompson, A. R., Moran, J. M., & Swenson Jr, G. W. 2017, *Interferometry and Synthesis in Radio Astronomy*, 3rd edn. (Springer Open)
- Trippe, S., Jung, T., Lee, J.-W., et al. 2023, arXiv e-prints, arXiv:2304.06482, doi: [10.48550/arXiv.2304.06482](https://doi.org/10.48550/arXiv.2304.06482)
- Vallado, D. 2006, *Fundamentals of Astrodynamics and Applications* (Microcosm Press)
- Zakhvatkin, M. V., Andrianov, A. S., Avdeev, V. Y., et al. 2020, *Advances in Space Research*, 798, doi: [10.1016/j.asr.2019.05.007](https://doi.org/10.1016/j.asr.2019.05.007)